Structure, Volume *25*

Supplemental Information

Structural Basis for the Inhibitory Effects of Ubistatins in the Ubiquitin-Proteasome Pathway

Mark A. Nakasone, Timothy A. Lewis, Olivier Walker, Anita Thakur, Wissam Mansour, Carlos A. Castañeda, Jennifer L. Goeckeler-Fried, Frank Parlati, Tsui-Fen Chou, Ortal Hayat, Daoning Zhang, Christina M. Camara, Steven M. Bonn, Urszula K. Nowicka, Susan Krueger, Michael H. Glickman, Jeffrey L. Brodsky, Raymond J. Deshaies, and David Fushman

Supplemental Information

Structural basis for the inhibitory effects of ubistatins in the ubiquitin-proteasome pathway

Mark A. Nakasone, Timothy A. Lewis, Olivier Walker, Anita Thakur, Wissam Mansour, Carlos A. Castañeda, Jennifer L. Goeckeler-Fried, Frank Parlati, Tsui-Fen Chou, Ortal Hayat, Daoning Zhang, Christina M. Camara, Steven M. Bonn, Urszula K. Nowicka, Susan Krueger, Michael H. Glickman, Jeffrey L. Brodsky, Raymond J. Deshaies, and David Fushman

Supplemental Figures

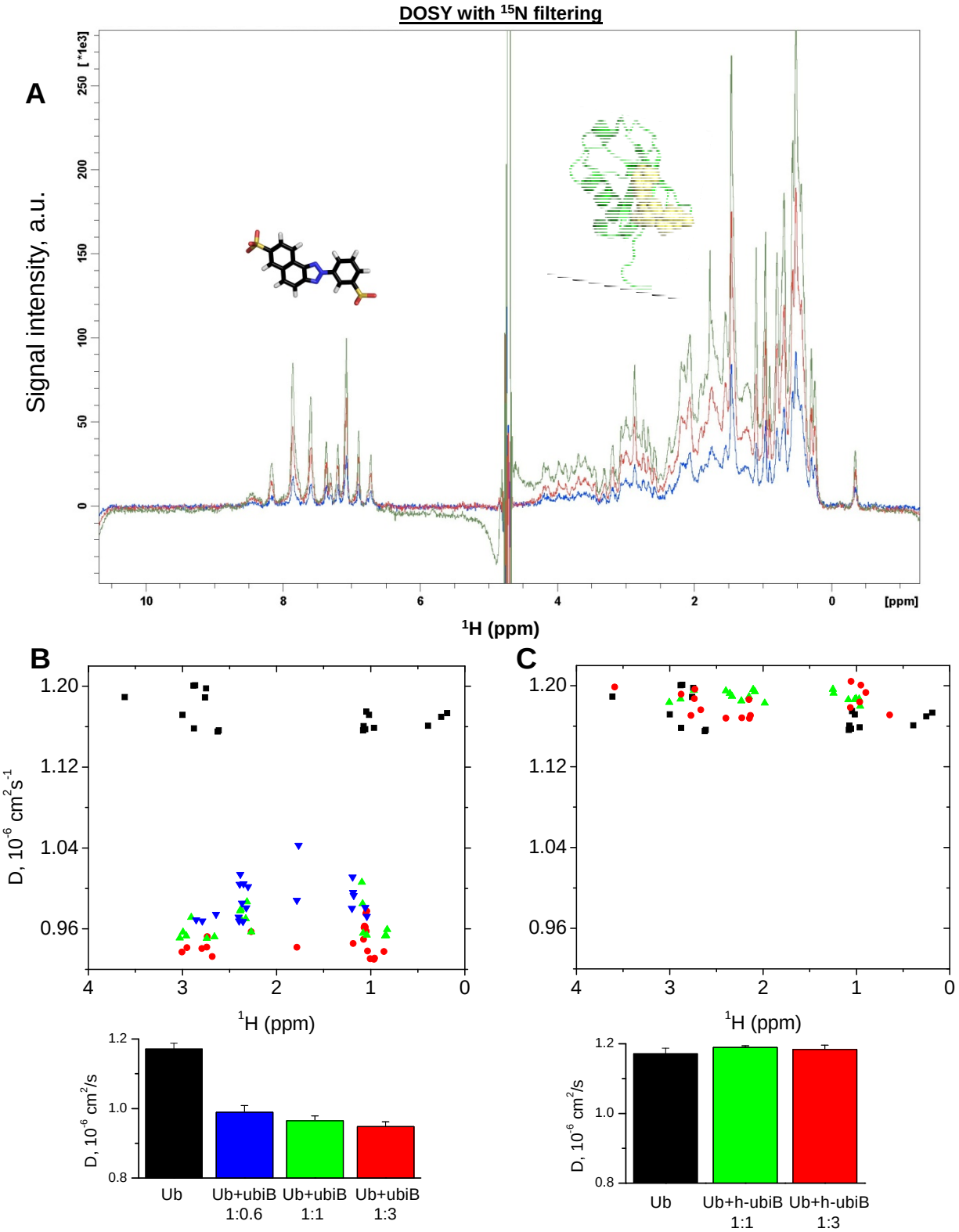

Figure S1, related to Figure 2. Changes in the translational diffusion coefficient of Ub upon binding to ubistatins. PFG-DOSY with ^{15}N filtering was applied at various points in titration of ^{15}N-labeled Ub with ubistatin compounds h-ubiB and ubiB. (**A**) Overlay of 1D spectra at differing gradient strengths in the same experiment shows robust signals from carbon-bonded protons in Ub and suppression of those from ^{15}N-bonded protons, allowing ^{1}H signals from h-ubiB to appear clearly (downfield from H_2O signal, left side). Translational

diffusion coefficients were determined using signals from Ub's aliphatic protons (0-4 ppm) with intensities well above the level of noise. (**B**) Ub exhibits a large decrease in translational diffusion coefficient upon addition of ubiB even below 1:1 ratio ([ubiB]:[Ub]=0.0 black squares, [ubiB]:[Ub]=0.6 blue triangles, [ubiB]:[Ub]=1.0 green triangles and [ubiB]:[Ub]=3.0 red circles). (**C**) In contrast to ubiB, h-ubiB does not cause a decrease in the translational diffusion coefficient across the titration range ([h-ubiB]:[Ub]=0.0 black squares, [h-ubiB]:[Ub]=1.0 green triangles, [h-ubiB]:[Ub]=3.0 red diamonds). The bar plots shown on the bottom of panels B and C show the mean value and standard deviation (error bars) of the diffusion coefficient determined from the individual signals (colored as the data points).

The diffusion coefficient of Ub decreased upon binding ubiB by a factor of 1.24±0.03. Because the translational diffusion coefficient is inversely proportional to the hydrodynamic radius of a molecule, this indicates an increase in the hydrodynamic radius by the same factor, which corresponds to an increase in the hydrodynamic volume by a factor of $(1.24\pm0.03)^3 \approx 2$. This is fully consistent with the model where two Ubs bind to the same ubiB molecule, forming a 2:1 complex.

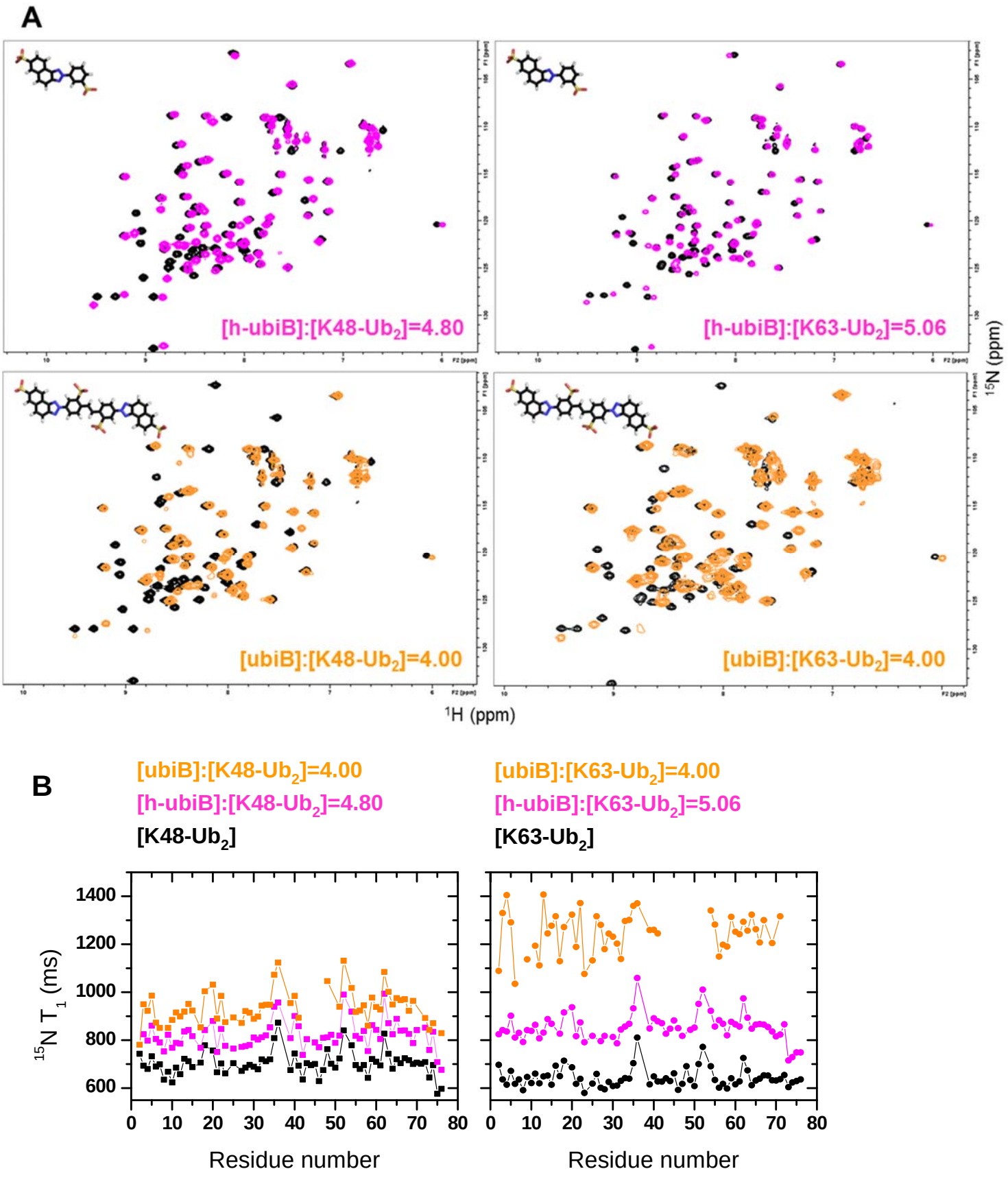

Figure S2, related to Figure 2. NMR characterization of h-ubiB and ubiB interactions with K48- Ub_2 and K63-Ub_2.

(**A**) Overlay of ^{1}H-^{15}N SOFAST-HMQC spectra of the distal Ub in K48-Ub_2 or K63-Ub_2 before the titration (black contours) and at the endpoint of titration with h-ubiB (magenta) or ubiB (orange).

(**B**) Oligomerization of dimeric Ub with ubiB. ^{15}N T_1 values for residues in K48-Ub_2 (left panel) and K63-Ub_2 (right panel) show a slight increase upon binding of h-ubiB (magenta) versus the unbound dimers (black). Residues in K48-Ub_2 in complex with ubiB (orange, left panel) exhibit ^{15}N T_1 values nearing the ^{15}N T_1 level for unbound K48-Ub_3 (~950 ms (Varadan et al., 2005)), while the ^{15}N T_1 values for K63-Ub_2 in complex with ubiB (orange, right panel) approach and even exceed the ^{15}N T_1 level of unbound K48-Ub_4 (see Table 1, main text).

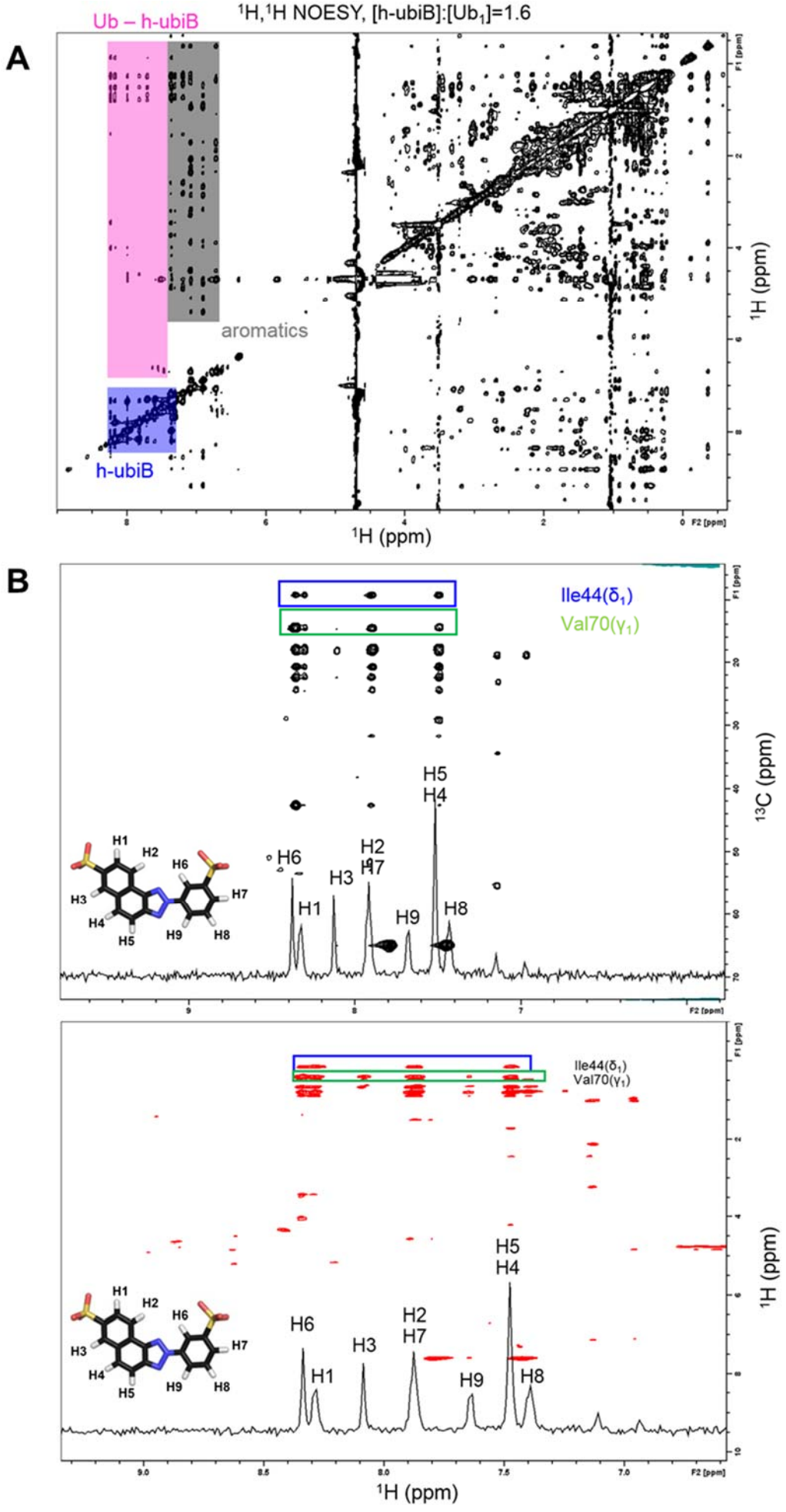
A
^{1}H,^{1}H NOESY, [h-ubiB]:[Ub$_1$]=1.6
Ub – h-ubiB
aromatics
h-ubiB
^{1}H (ppm)
^{1}H (ppm)
B
Ile44(δ$_1$)
Val70(γ$_1$)
H1
H2
H3
H4
H5
H6
H7
H8
H9
^{13}C (ppm)
Ile44(δ$_1$)
Val70(γ$_1$)
^{1}H (ppm)
^{1}H (ppm)

Figure S3, related to Figure 3. NMR characterization of the structure of Ub:h-ubiB complex using NOESY experiments.

(**A**) ^{15}N filtered ^{1}H,^{1}H-NOESY spectrum of ^{15}N Ub + h-ubiB sample shows a network of diagnostic NOEs in the h-ubiB:Ub complex.

(**B**) Intermolecular NOEs between residues in Ub and h-ubiB protons. 2D slices (top: ^{13}C-^{1}H, bottom: ^{1}H-^{1}H) from ^{13}C-edited/filtered 3D ^{1}H-^{1}H NOESY spectrum. Methyl groups of Ile44 and Val70 show strong NOEs to several protons in h-ubiB.

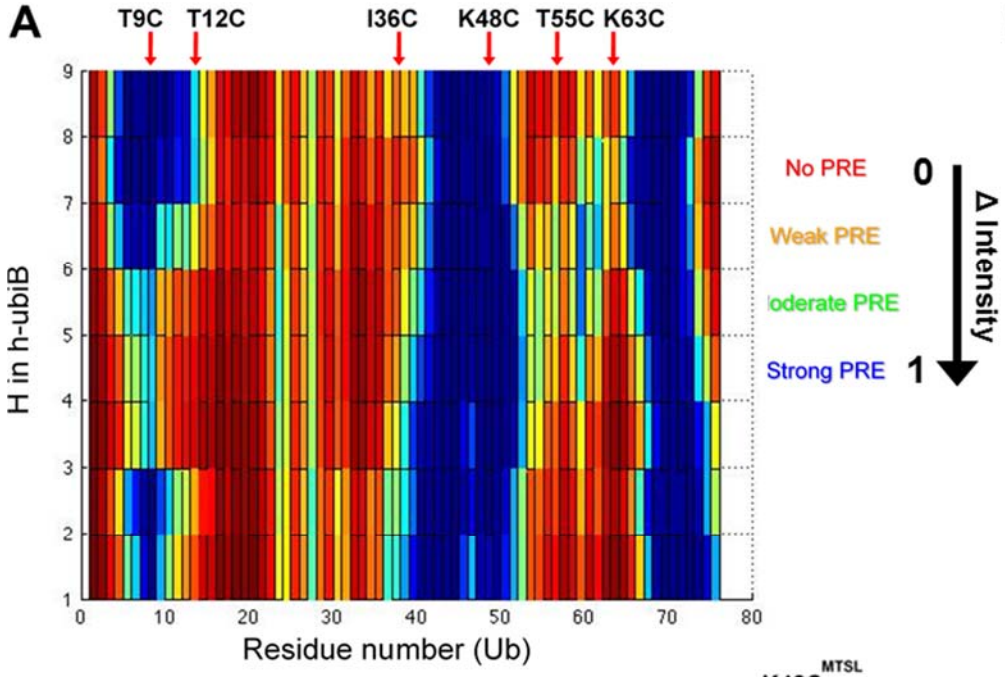
A
T9C
T12C
I36C
K48C
T55C
K63C
H in h-ubiB
Residue number (Ub)
No PRE
Weak PRE
oderate PRE
Strong PRE
0
1
Δ Intensity

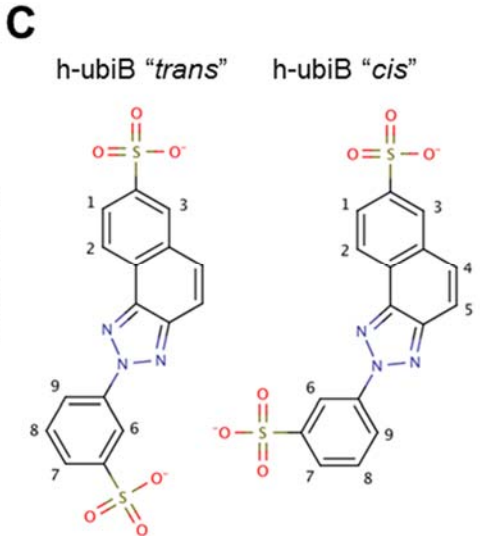
C
h-ubiB "trans"
h-ubiB "cis"

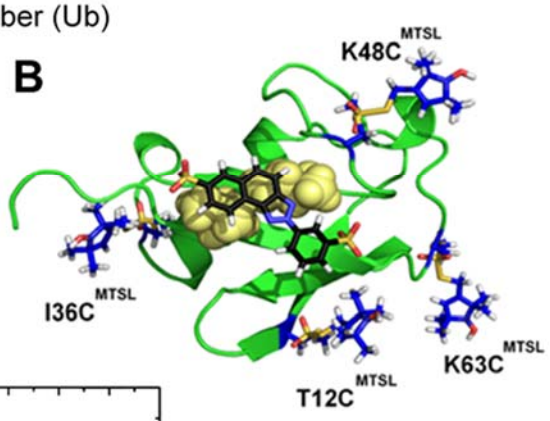
B
K48C MTSL
I36C MTSL
T12C MTSL
K63C MTSL

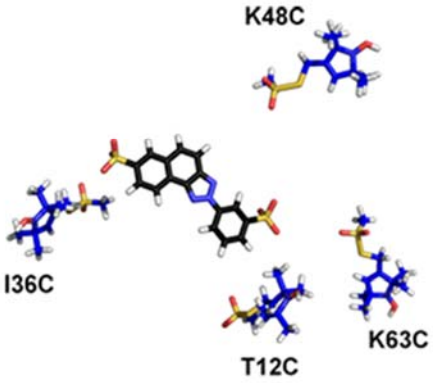
K48C
I36C
T12C
K63C

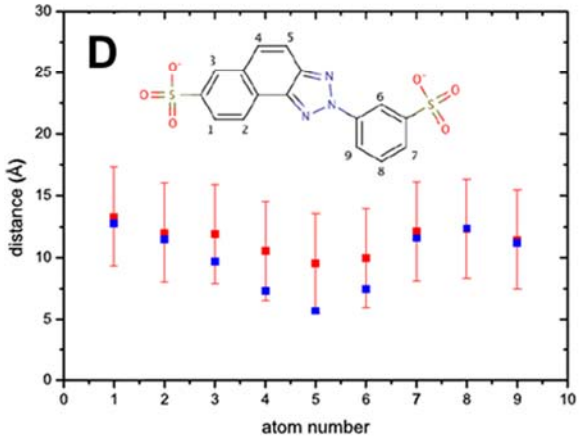
D
distance (Å)
atom number

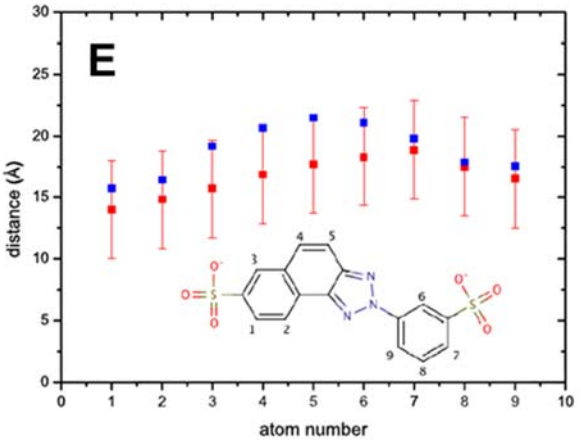
E
distance (Å)
atom number

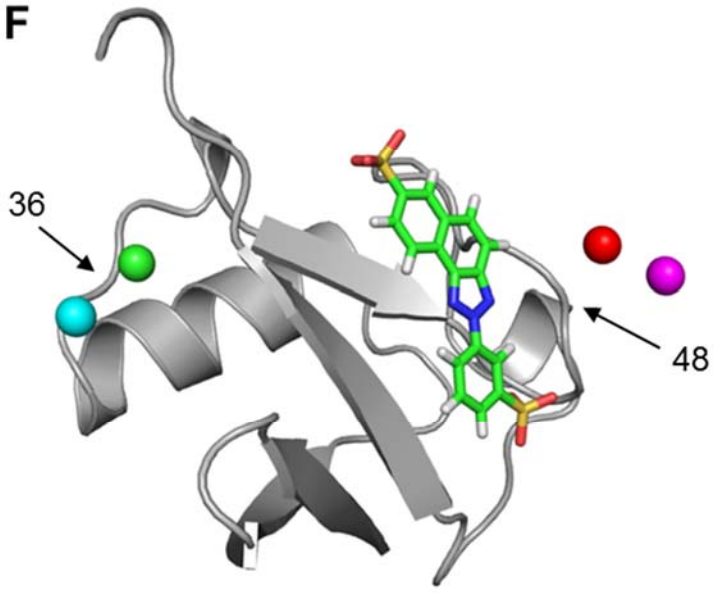
F
36
48

Figure S4, related to Figure 3. NMR characterization of the structure of Ub:h-ubiB complex using paramagnetic spin labeling.

(**A**) Simulation of the PRE effect on the nine protons in h-ubiB caused by placing of MTSL on any residue in Ub. The calculation was based on the NOE-derived models of the Ub:h-ubiB complex.

(**B**) Ub cysteine mutants position MTSL around h-ubiB on the surface of Ub.

(**C**) The two possible conformations of the h-ubiB compound. The geometry of the h-ubiB compound was optimized by using the ORCA package (Neese, 2008). Since electron correlation contribution becomes more significant for aromatic compounds, we used density functional theory (DFT) to minimize the energy of h-ubiB. We used a combination of B3 exchange (Becke, 1998) and LYP correlation (Lee et al., 1988) functionals and a 6-31G** basis set. Energy minimization of the two possible conformations of the h-ubiB compound revealed that the *trans* conformation has a total energy lower by 10 kJ/mol than the *cis* conformation. The *trans* conformation was subsequently used for the docking process in the h-ubiB:Ub structure calculation.
The corresponding ligand topology file was created by using the PRODRG server (Schuttelkopf and van Aalten, 2004) whereas Mulliken charges were computed at the same level of theory and included in the topology file.

(**D-E**) Comparison of the experimental and back-calculated distances between h-ubiB protons and the unpaired electron of MTSL corresponding to PRE experiments when MTSL was attached to Cys48 (**D**) or Cys36 (**E**) of Ub. The red squares represent the distances derived from the experimental PRE data; the error bars represent the upper and lower boundaries of ±4 Å for the MTSL position to account for the flexibility of MTSL. Blue squares represent the back-calculated distances from the best structure of the modeled h-ubiB:Ub complex.

(**F**) The reconstructed positions of MTSL's unpaired electron are shown as spheres superimposed on the cartoon representation of the structure of the Ub:h-ubiB complex. Red and cyan spheres represent the MTSL's position reconstructed from the PREs measured in Ub, when MTSL was attached to Cys48 or Cys36, respectively. The corresponding positions of MTSL reconstructed from the PREs measured in h-ubiB using SLfit (Ryabov and Fushman, 2006) are shown as magenta and green spheres, respectively, for Ub^{K48C} and Ub^{I36C}. The locations of residues 36 and 48 in Ub are indicated. The good agreement between the results derived from the PREs measured in h-ubiB and in Ub supports the structure of the Ub:h-ubiB complex.

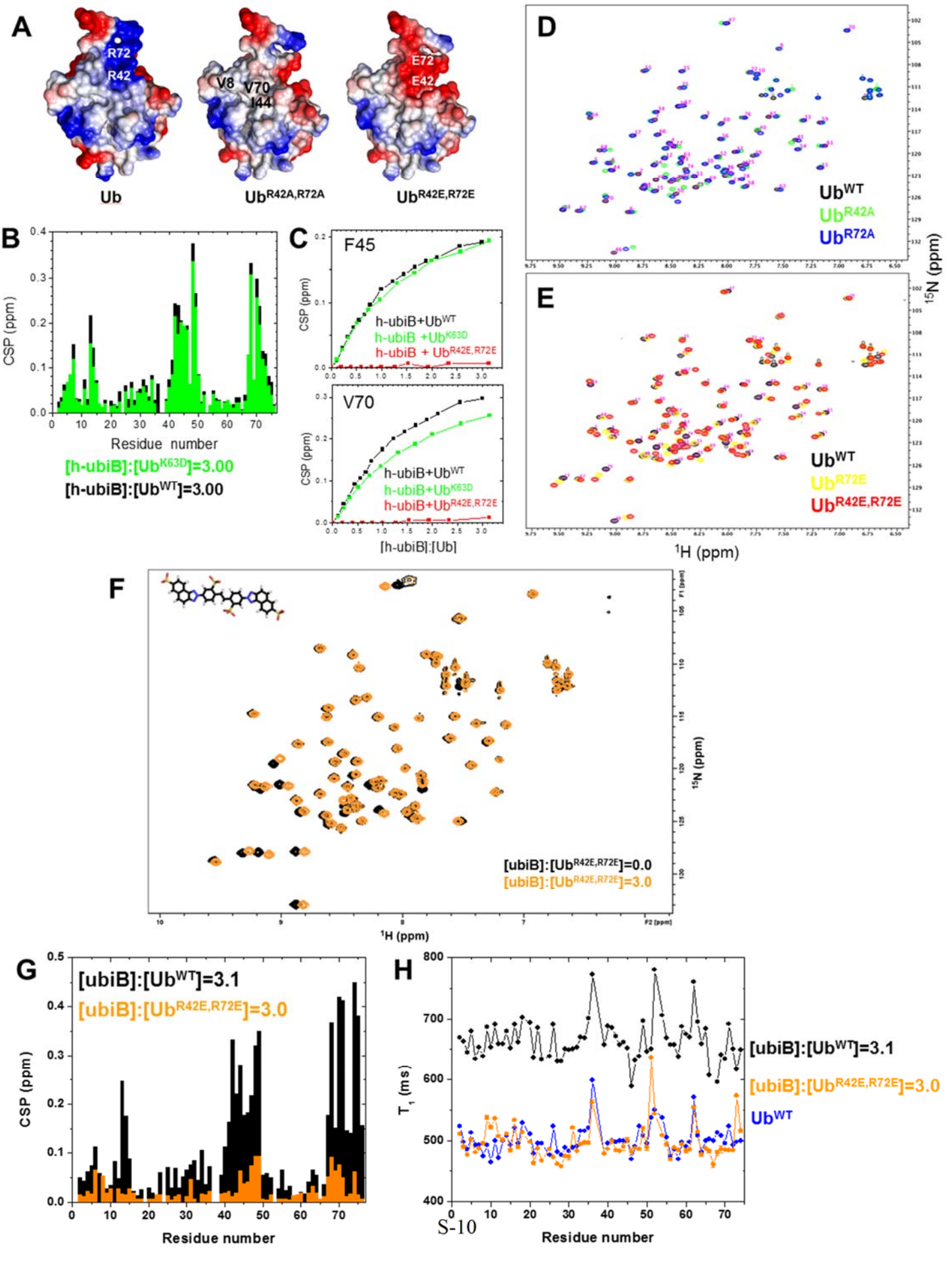
A
R72
R42
V8
V70
I44
E72
E42
Ub
Ub^R42A,R72A
Ub^R42E,R72E
B
CSP (ppm)
Residue number
[h-ubiB]:[Ub^K63D]=3.00
[h-ubiB]:[Ub^WT]=3.00
C
F45
V70
CSP (ppm)
h-ubiB+Ub^WT
h-ubiB +Ub^K63D
h-ubiB + Ub^R42E,R72E
h-ubiB+Ub^WT
h-ubiB+Ub^K63D
h-ubiB+Ub^R42E,R72E
[h-ubiB]:[Ub]
D
Ub^WT
Ub^R42A
Ub^R72A
15N (ppm)
E
Ub^WT
Ub^R72E
Ub^R42E,R72E
1H (ppm)
F
[ubiB]:[Ub^R42E,R72E]=0.0
[ubiB]:[Ub^R42E,R72E]=3.0
15N (ppm)
1H (ppm)
G
[ubiB]:[Ub^WT]=3.1
[ubiB]:[Ub^R42E,R72E]=3.0
CSP (ppm)
Residue number
H
T1 (ms)
[ubiB]:[Ub^WT]=3.1
[ubiB]:[Ub^R42E,R72E]=3.0
Ub^WT
Residue number

Figure S5, related to Figure 3. The results of site-directed mutagenesis.
(**A**) Electrostatic surface representation of Ub^{WT}, $Ub^{R42A,R72A}$, and $Ub^{R42E,R72E}$: the R42E,R72E mutation transitions the cationic region adjacent to Ub's hydrophobic patch to anionic.

(**B**) Changing the bulk charge of Ub by mutations away from the h-ubiB binding site does not adversely impact binding. Residue-specific CSPs from titration of the Ub^{K63D} variant (green) with h-ubiB are nearly identical to those for Ub^{WT} (black).

(**C**) Representative titration curves for F45 and V70 further support that binding of h-ubiB to Ub^{K63D} (green) occurs as to Ub^{WT} (black). For comparison the titration curve for the $Ub^{R42E,R72E}$ (red) represents abolishment of binding.

(**D**) Overlay of ^{1}H-^{15}N SOFAST-HMQC spectra of Ub^{WT} (black), Ub^{R42A} (green), and Ub^{R72A} (blue) shows gradual titration of chemical shifts of Ub residues as a result of changes in the electrostatic potential upon R→A substitutions, but with no dramatic changes in the signals positions or spread, thus indicating that the 3-D structure of Ub remains intact. Numbers at each amide signal of Ub^{WT} indicate the corresponding residues.

(**E**) Overlay of ^{1}H-^{15}N SOFAST-HMQC spectra of Ub^{WT} (black), Ub^{R72E} (yellow), and $Ub^{R42E,R72E}$ (red) shows gradual titration of chemical shifts of Ub residues as a result of changes in the electrostatic potential upon R→E substitutions, but with no dramatic changes in the signals positions or spread, thus indicating that the 3-D structure of Ub remains intact even for the $Ub^{R42E,R72E}$ variant. Numbers at each amide signal of Ub^{WT} indicate the corresponding residues.

(F-H) The R42E,R72E mutation in Ub dramatically reduced ubiB binding. (**F**) ^{1}H-^{15}N SOFAST-HMQC signals from $Ub^{R42E,R72E}$ at the titration endpoint (orange) do not exhibit attenuations or wide-spread CSPs as in Ub^{WT}. (**G**) CSPs at titration endpoints for $Ub^{R42E,R72E}$ (orange) and Ub^{WT} (black) demonstrate that the anionic substitution greatly reduced binding of ubiB. (**H**) ^{15}N T_1 values in $Ub^{R42E,R72E}$ at titration endpoint (orange) did not increase as in Ub^{WT} (black) and remained essentially the same as in the unbound Ub^{WT} (blue): 493 ± 27 ms (averaged over residues in structured regions of $Ub^{R42E,R72E}$).

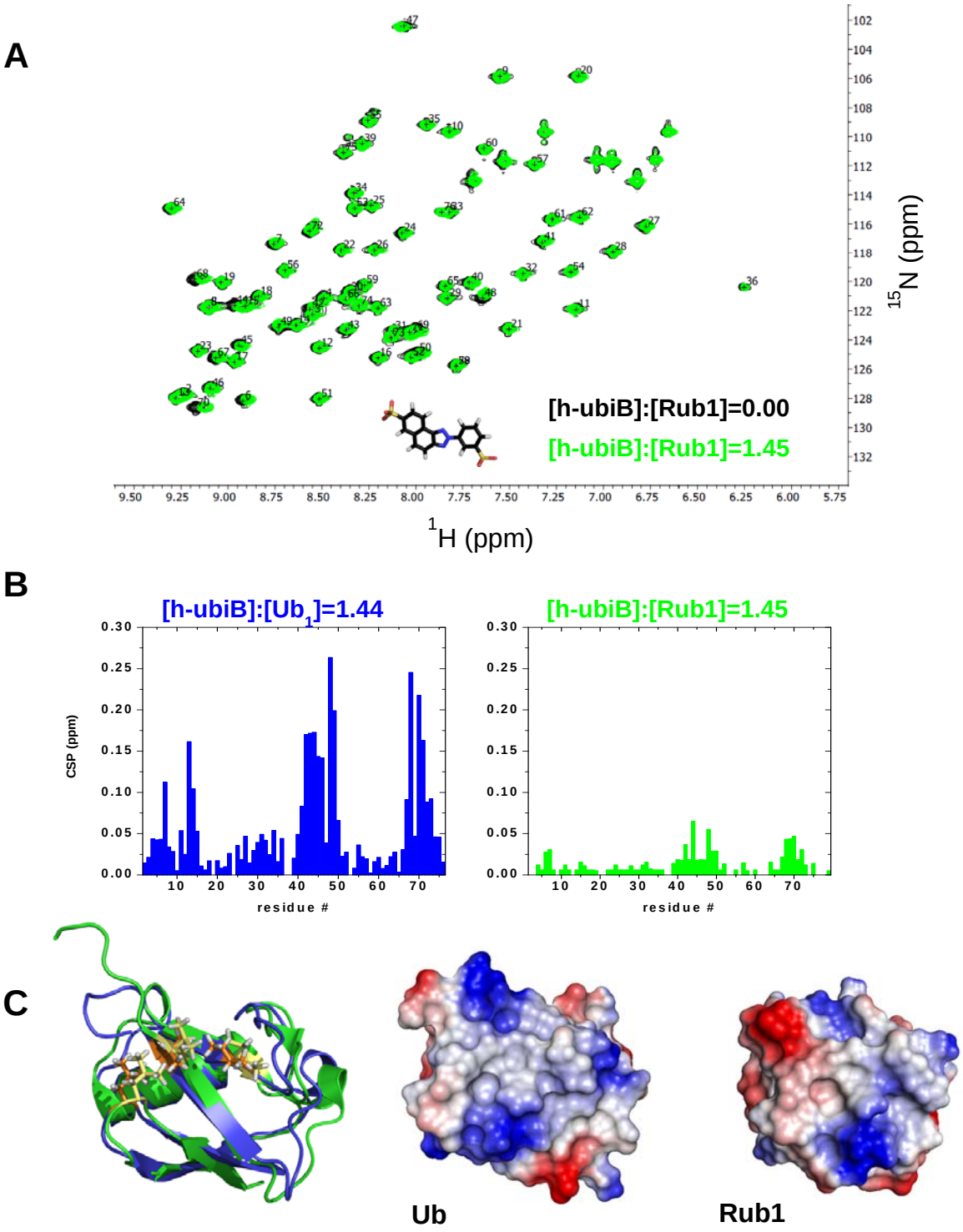

Figure S6, related to Figure 3. Rub1 (yeast orthologue of human Nedd8), the closest kin of Ub carrying the R72T mutation (Singh et al., 2012), fails to bind h-ubiB. (**A**) Overlay of ^{1}H-^{15}N SOFAST-HMQC spectra of Rub1 before (black) and after addition (green) of h-ubiB at a 1.45:1 molar ratio. (**B**) Comparison of chemical shift perturbations in Ub (left) and Rub1 (right) upon addition of h-ubiB at a similar (1.45:1) molar ratio. (**C**) Comparison of the 3-D structures (Ub in green, Rub1 in blue) and surface electrostatic potentials of Ub and Rub1. For the purposes of comparison of the surfaces, the last three C-terminal residues were removed from each protein.

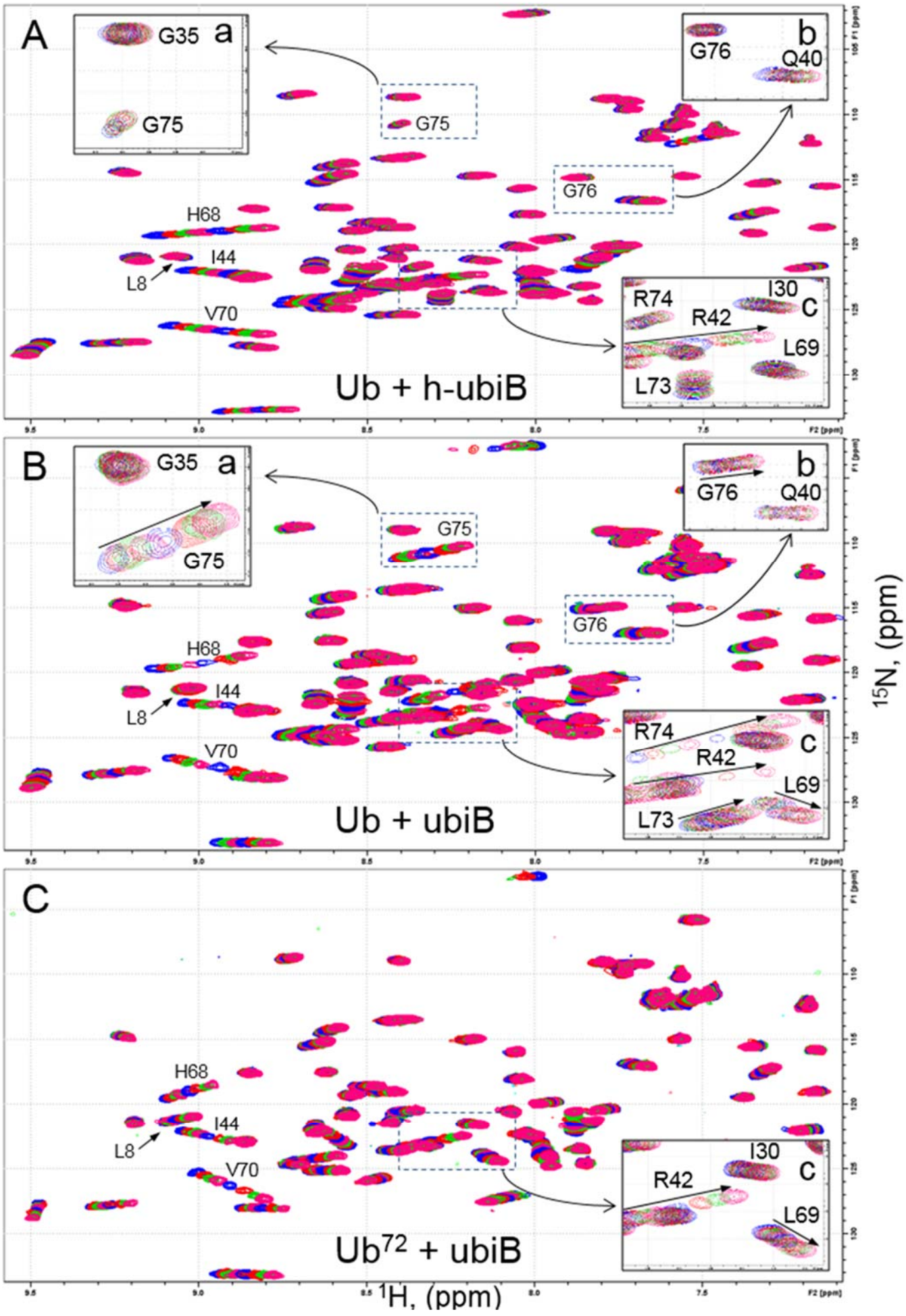
A
G35
a
G75
G75
b
G76
Q40
G76
H68
I44
L8
V70
R74
I30
c
R42
L69
L73
Ub + h-ubiB
B
G35
a
G75
G75
b
G76
Q40
G76
H68
I44
L8
V70
R74
c
R42
L69
L73
Ub + ubiB
C
H68
I44
L8
V70
I30
c
R42
L69
Ub72 + ubiB
15N, (ppm)
1H, (ppm)

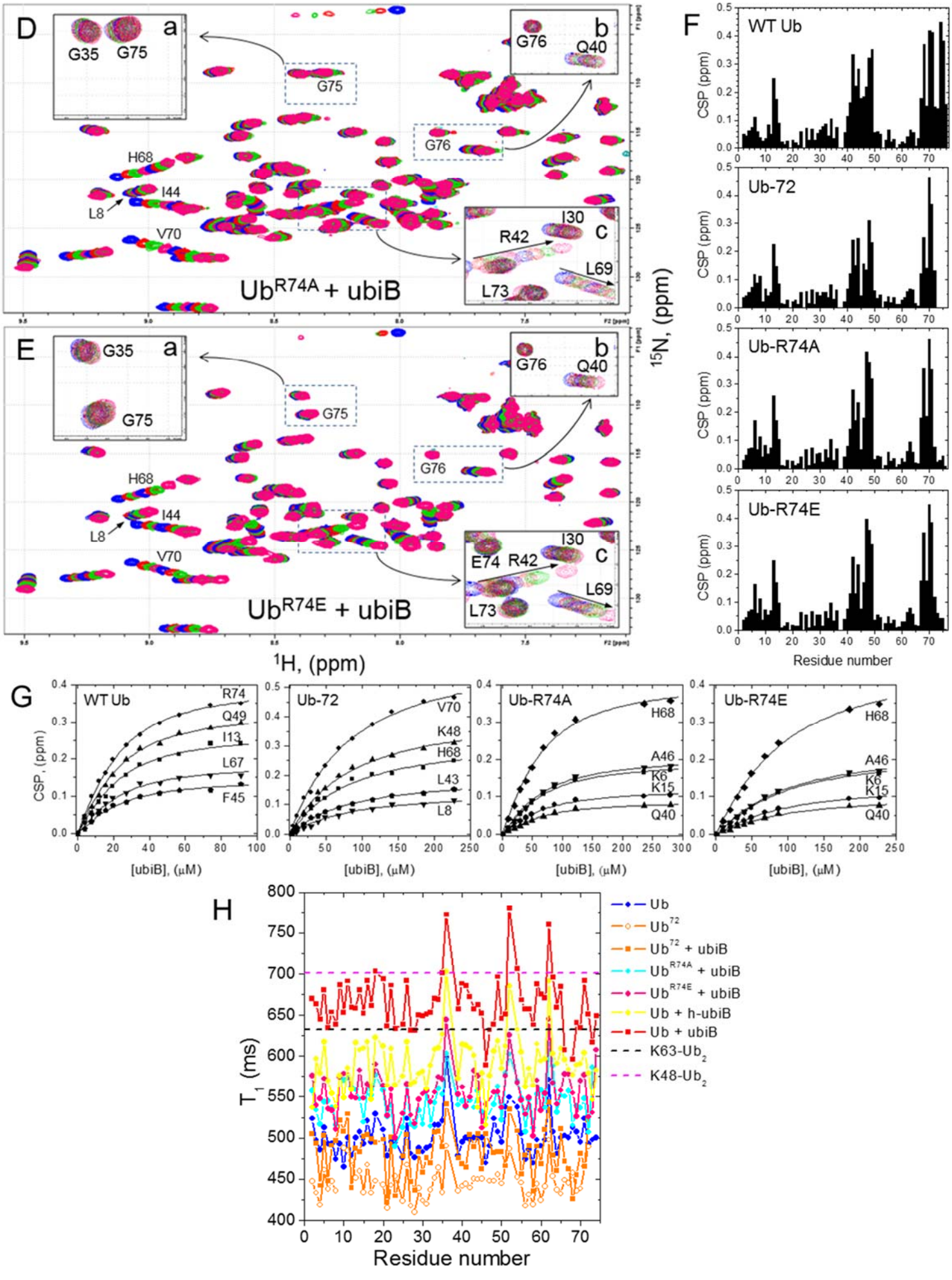
D
a
G35
G75
b
G76
Q40
G75
G76
H68
I44
L8
V70
I30
R42
c
L69
L73
Ub^R74A + ubiB
E
a
G35
G75
b
G76
Q40
G75
G76
H68
I44
L8
V70
I30
E74
R42
c
L69
L73
Ub^R74E + ubiB
15N, (ppm)
1H, (ppm)
F
WT Ub
Ub-72
Ub-R74A
Ub-R74E
CSP (ppm)
Residue number
G
WT Ub
R74
Q49
I13
L67
F45
Ub-72
V70
K48
H68
L43
L8
Ub-R74A
H68
A46
K6
K15
Q40
Ub-R74E
H68
A46
K6
K15
Q40
CSP, (ppm)
[ubiB], (μM)
H
T1 (ms)
Residue number
Ub
Ub72
Ub72 + ubiB
UbR74A + ubiB
UbR74E + ubiB
Ub + h-ubiB
Ub + ubiB
K63-Ub2
K48-Ub2

Figure S7, related to Figure 4. Comparison of h-ubiB and ubiB binding to Ub and of ubiB binding to Ub^{WT} and Ub variants.

(**A-E**) Overlay of ^{1}H-^{15}N SOFAST-HMQC NMR spectra of Ub^{WT} (**A-B**) and Ub variants, Ub^{72} (**C**), Ub^{R74A} (**D**) and Ub^{R74E} (**E**) in the course of their titration with h-ubiB (**A**) or ubiB (**B-E**), as indicated. The insets (a, b, c) zoom on the spectral regions containing signals from C-terminal residues G75 (a), G76 (b), and R72, L73, and R74 (c), as indicated. Signals corresponding to the hydrophobic patch residues L8, I44, H68, and V70 are also indicated by residue numbers. The spectra of free protein are shown in blue contours, the titration end-point spectra are in red.

(**F**) CSPs in Ub^{WT}, Ub^{72}, Ub^{R74A}, and Ub^{R74E}, as indicated, as a function of residue number at the titration endpoint with ubiB.

(**G**) Representative titration curves for ubiB binding to Ub^{WT}, Ub^{72}, Ub^{R74A}, and Ub^{R74E}, as indicated. The symbols show CSPs for indicated residues, the lines correspond to the global fit of all residues to Equations S2-S3 (see Method Details (STAR Methods)). The corresponding K_d values are in Table 2 (main text).

(**H**) Comparison of ^{15}N T_1 values for Ub^{WT} (red), Ub^{72} (orange), Ub^{R74A} (cyan), and Ub^{R74E} (pink) at the endpoint of titration with ubiB. Also shown, as the reference, are T_1 values for free Ub (blue circles), free Ub^{72} (open orange circles), and for Ub in complex with h-ubiB (yellow). Also shown, for comparison, are average ^{15}N T_1 values for unbound K48-Ub_2 and K63-Ub_2 (horizontal dashed lines colored magenta and black, respectively) to illustrate that the ^{15}N T_1 values for Ub^{WT} in complex with ubiB are comparable to the ^{15}N T_1 values for unbound Ub_2 (see also Figure 2I, main text).

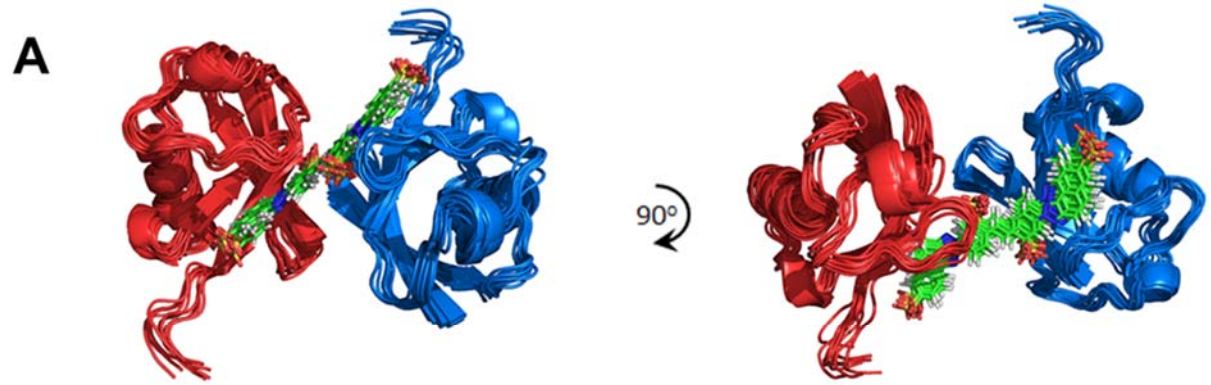
A
90°

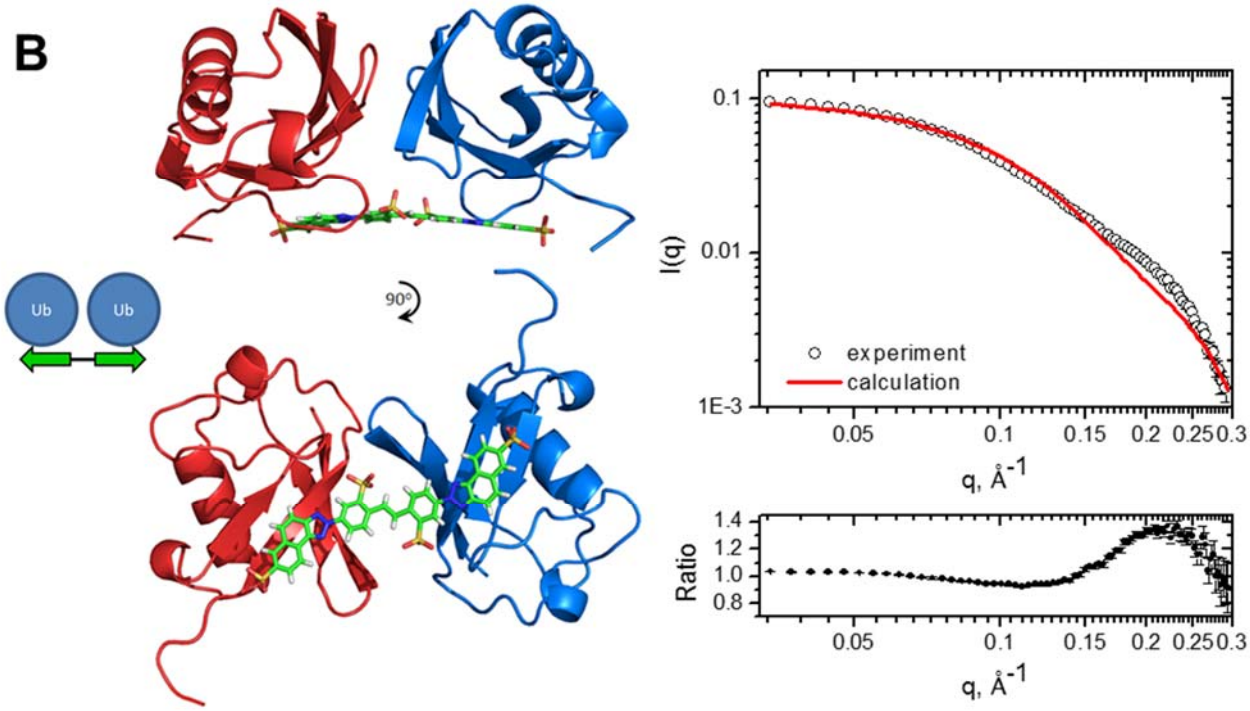
B
Ub
Ub
90°
I(q)
0.1
0.01
1E-3
experiment
calculation
0.05
0.1
0.15
0.2
0.25
0.3
q, Å-1
Ratio
1.4
1.2
1.0
0.8
0.05
0.1
0.15
0.2
0.25
0.3
q, Å-1

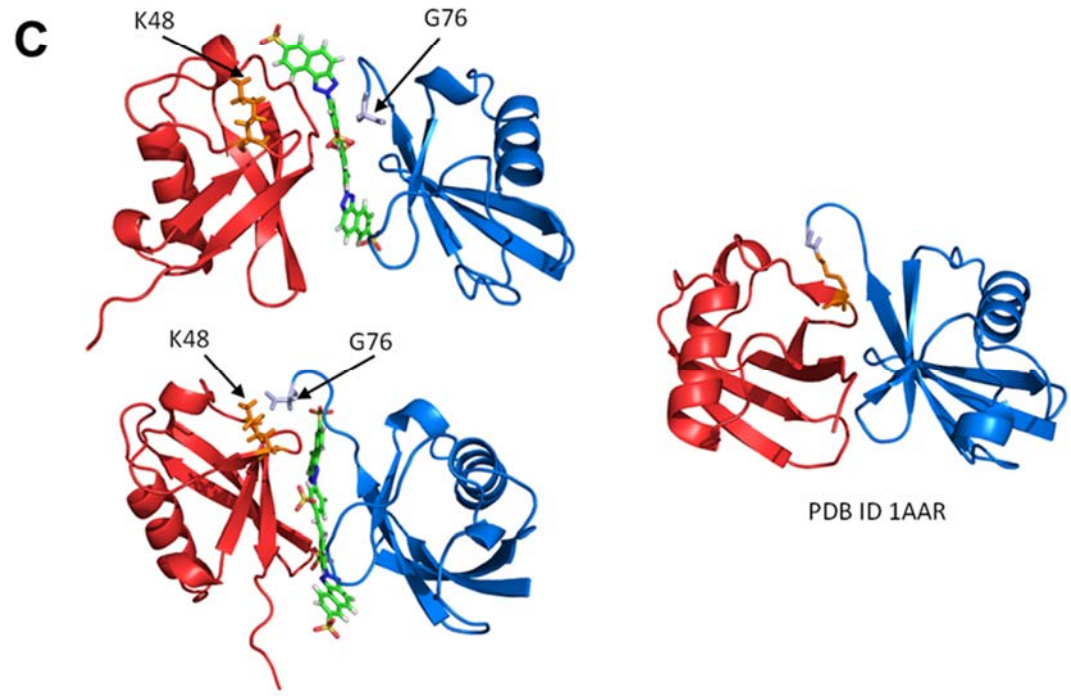
C
K48
G76
K48
G76
PDB ID 1AAR

Figure S8, related to Figure 5. Characterization of ubiB complexes with Ub.

(**A**) Ten structures of the ternary Ub:ubiB:Ub complex from the top-scoring cluster of HADDOCK-generated models, after the flexible docking step.

(**B**) HADDOCK-generated model of the ternary Ub:ubiB:Ub complex with both Ubs positioned on the same face of ubiB. The plots on the right show comparison of the SANS profile computed for this structure with the experimental data, Ratio = $I(q)^{exp}/I(q)^{calc}$. The error bars represent standard errors in $I(q)^{exp}$. This structure demonstrates that ubiB can accommodate two Ub molecules on one face (as also shown in the cartoon on the left). 142 out of the 2000 structures generated at the HADDOCK rigid body docking step had a similar arrangement with both Ubs placed on the same face of ubiB. None of the final 200 HADDOCK structures showed this arrangement.

(**C**) Representative structures extracted from the 50,000 snapshots of a 2 μs MD simulation trajectory of the ubiB:2xUb complex, showing compact structures, where the C-terminal G76 (light blue) of one Ub is positioned close to K48 (orange) of another Ub. Shown on the right, for comparison, is the crystal structure of the closed state of K48-linked Ub_2 (PDB ID: 1AAR). Among the 50,000 snapshots analyzed we found compact arrangements with one or both Ubs positioned somewhat closer to the center of ubiB compared to the starting structure (Figure 5D, main text), although there was no further improvement in the already excellent agreement with the SANS data.

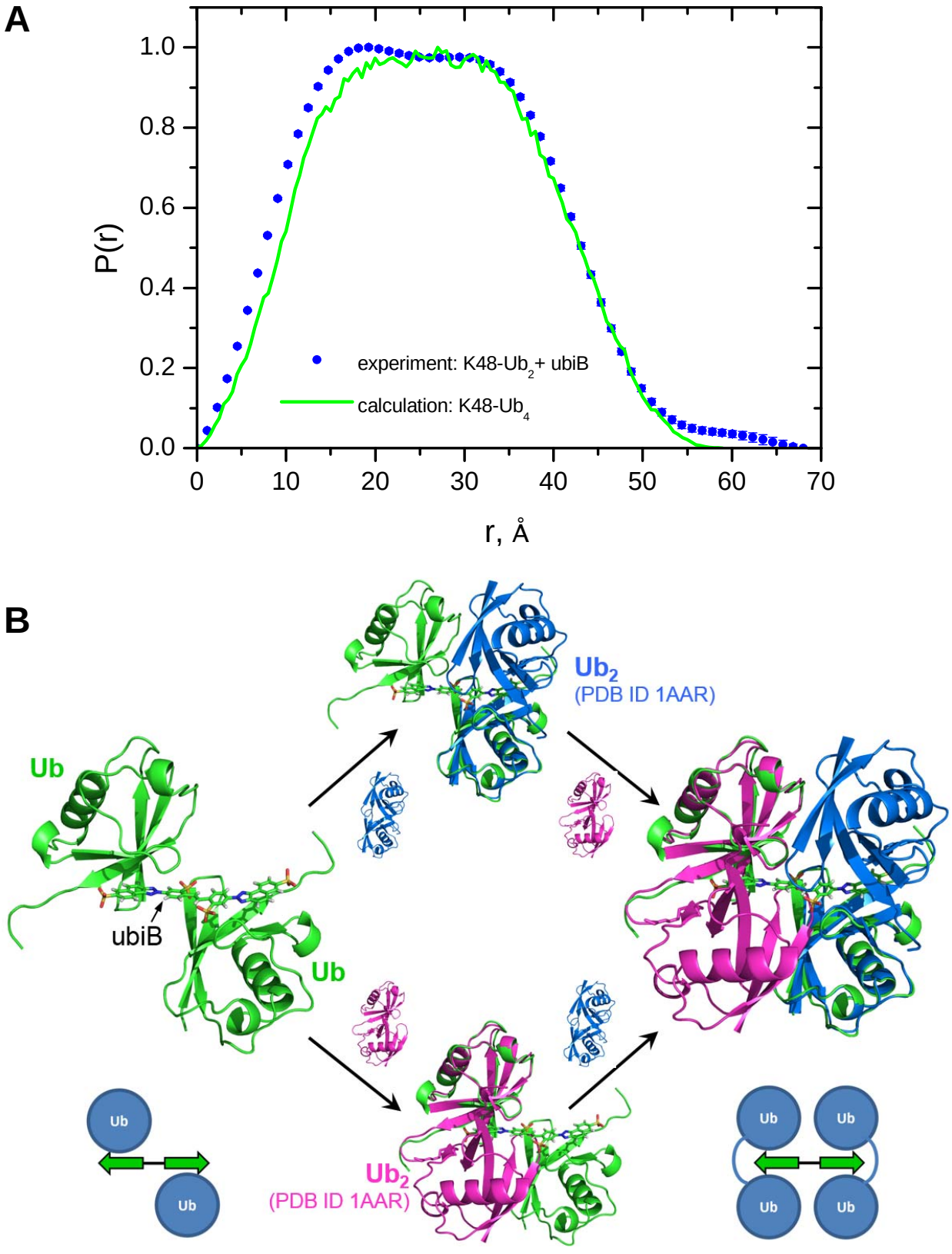

Figure S9, related to Figure 5. Characterization of ubiB complexes with K48-Ub2.

(A) Comparison of the pair distribution function, *P*(*r*), derived from SANS measurements for K48-Ub2 in complex with ubiB (blue circles) with the *P*(*r*) (green line) calculated directly from the crystal structure of the

closed state of K48-Ub_4 (PDB ID 2O6V (Eddins et al., 2007)). The error bars represent standard errors in the $P(r)$ values derived from SANS data. The measured R_g for K48-Ub_2+ubiB (20.1±0.1 Å) matches the R_g value (20.27 Å) predicted from the K48-Ub_4 structure.

(B) Structural illustration of how two K48-Ub_2 molecules could form a compact tetra-Ub-like complex with a single ubiB molecule. Shown on the left is the complex, Ub:ubiB:Ub, of two Ub molecules (green) with ubiB, from Figure 5D. Shown in the middle panel are superimpositions of the crystal structure (PDB ID 1AAR) of the closed form of K48-Ub_2 with the Ub:ubiB:Ub structure. Here the distal Ub of K48-Ub_2 is aligned with either Ub molecule from Ub:ubiB:Ub. Shown on the right is a simultaneous superposition of two K48-Ub_2 molecules with the Ub:ubiB:Ub structure; each alignment is the same as in the middle panel including the coloring of the Ub_2 molecules. The arrows are intended to guide the reader through the consecutive alignment steps. The pictograms on the bottom are schematic drawings of such complexes from Figure 5E.

Note that while our NMR and SANS data clearly indicate that K48-Ub_2 forms a 2:1 complex with ubiB, we cannot rule out that a fraction of K48-Ub_2 binds ubiB with a 1:1 stoichiometry, possibly utilizing a binding mode similar to that observed for the Ub:ubiB:Ub complex. For example, the ≈40% increase in $I(q\approx0)$ of the di-Ub upon addition of ubiB is smaller than a ≈100% increase expected in the case of complete dimerization. Also, the average ^{15}N T_1 value (942 ms) of K48-Ub_2 in the presence of ubiB is somewhat smaller than the corresponding value for tetra-Ub (1124 ms (Varadan et al., 2005)). Together, these observations suggest that not all Ub_2 molecules in the Ub_2+ubiB sample form dimers or higher-stoichiometry aggregates with ubiB. Thus we assume that a fraction of the Ub_2 chains are either unbound or form a 1:1 complex, possibly resembling those shown in Figure S8C.

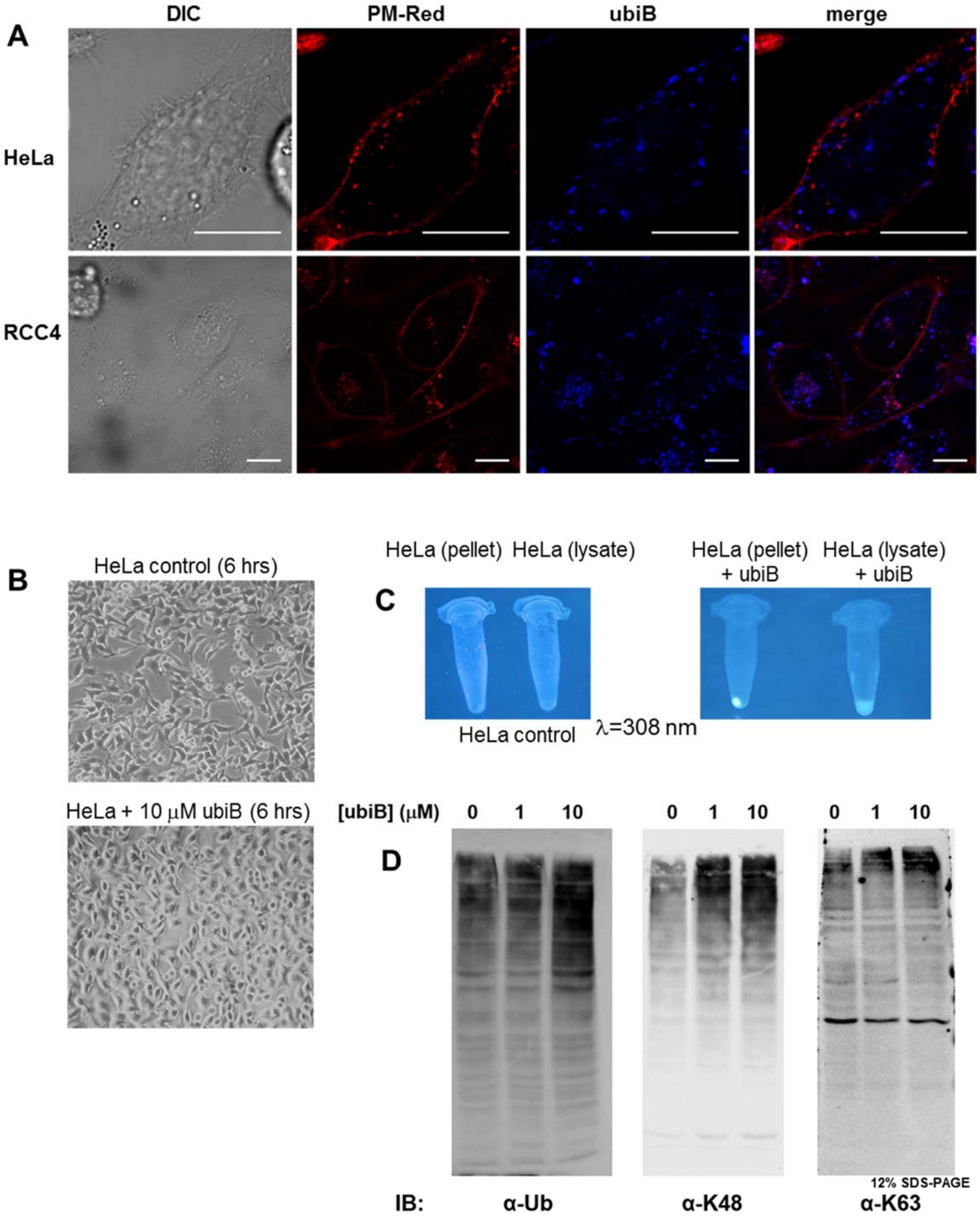
A
DIC
PM-Red
ubiB
merge
HeLa
RCC4
B
HeLa control (6 hrs)
HeLa + 10 μM ubiB (6 hrs)
C
HeLa (pellet)
HeLa (lysate)
HeLa (pellet) + ubiB
HeLa (lysate) + ubiB
HeLa control
λ=308 nm
D
[ubiB] (μM)
0 1 10
0 1 10
0 1 10
12% SDS-PAGE
IB:
α-Ub
α-K48
α-K63

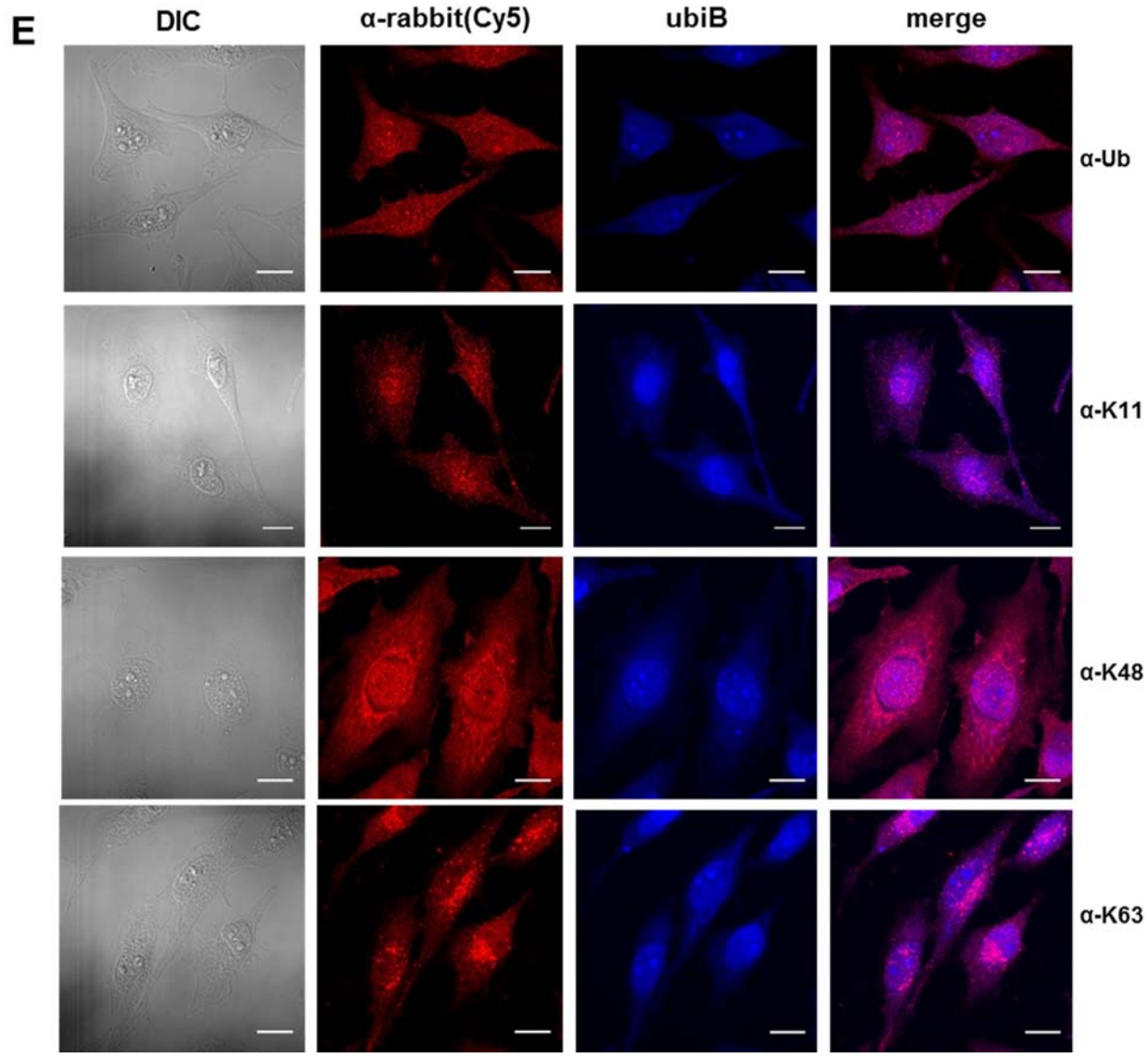

Figure S10, related to Figure 7. Internalization of ubiB in human cancer cells.

(**A**) Live cell imaging of HeLa (top row) and RCC4 (bottom row) cells shows signals from ubiB (blue) and the plasma membrane (red). Images in the left column were obtained using differential interface contrast (DIC) microscopy. White scale bars = 15 μm. For details see Method Details (STAR Methods).

(**B**) Six hour treatment with ubiB allows wide distribution within cells, yet does not alter their normal morphology. Comparison of wide-field microscopy images of ubiB-treated HeLa cells (bottom) with untreated HeLa cells (top) confirms their normal morphology.

(**C**) After lysis, excitation with a 308 nm lamp shows a clear fluorescent signal from ubiB in both the supernatant and pelleted cell debris of ubiB-treated HeLa cells.

(**D**) Following 6 hr treatment with 0 μM, 1 μM, or 10 μM ubiB, HeLa cells were lysed in RIPA buffer and analyzed with the indicated antibodies on a 12% SDS-PAGE gel. Total protein content was determined using Bradford assay to ensure equal loading.

(**E**) Following treatment with ubiB HeLa cells were fixed, permeabilized, and immunostained with the indicated primary antibody and visualized with the same fluorescent secondary antibody (red). The fluorescence signal of ubiB (blue) is retained. White scale bars = 15 μm.

Supplemental Tables

Table S1, related to Figure 1C. The effect of ubistatin variants on the DUB activity of Rpn11.

Compound	% Rpn11 Inhibition[a]	IC_{50}[b] (μM)
ubiB	78.7 ± 3.7	0.9 ± 0.1
1	34.0 ± 6.7	20 ± 2
2	52.0 ± 6.1	5.7 ± 0.7
3	85 [c]	35 ± 8
3 (sodium salt)	N.D.	23 ± 4
4 (sodium salt)	30.0 ± 11.1	N.D.
5	60 [c]	20 ± 1
6	5 [c]	N.D.
7	0	N.D.
8	N.D.	4.6 ± 0.5
9 h-ubiB	3.5 ± 6.7	N.D.
10	-2.1 ± 1.4	N.D.
11	3.5 ± 6.7	N.D.

[a] Compounds were tested at 10 μM in duplicate, except for ubiB (n=6). Shown are mean ± standard deviation.
[b] Measurements were carried out in quadruplicate, and variance is expressed as the standard deviation. N.D., not determined.
[c] Measurement error is unavailable.

Table S2, related to Figure 1D. Relative inhibition of CFTR ubiquitination by the ubistatin derivatives. Signal from ^{125}I-Ub (endpoint measurement) quantitated for the *in vitro* ubiquitination of CFTR (see Figure 1 in main text). The extent of CFTR ubiquitination in the DMSO control reactions was set to 100%. The data represent the mean and standard deviation of at least 3 determinations.

Compound	% CFTR Ubiquitination
DMSO	100
Ubistatin B	18 ± 2
8	40 ± 3
9	100 ± 7
10	100 ± 12
1	53 ± 16
2	29 ± 13
11	100 ± 4
3	100 ± 10
4	59 ± 15
7	53 ± 13
6	100 ± 3

Table S3, related to Figure 3. HADDOCK constraints used in the modeling of the Ub:h-ubiB complex

Ambiguous restraints

Ub	
Active residues	42,44,47,68
Passive residues	70
Flexible segments	8-14;
Fully flexible segments	72-76; 35-37; 46-50

h-ubiB	
Active residues	H1-H9
Fully flexible segments	Whole h-ubiB

Unambiguous restraints

NOE-derived distances

Ub		h-ubiB	Distance (Å)
Residue	atom	atom	
44	Hδ	H2	3.5 ± 2
44	Hδ	H3	3.6 ± 2
44	Hδ	H1	3.0 ± 2
44	Hδ	H6	2.8 ± 2
44	Hγ	H6	2.4 ± 2
44	Hγ	H1	2.9 ± 2
44	Hγ	H3	3.2 ± 2
44	Hγ	H9	4.0 ± 2
70	Hγ	H2	3.4 ± 2
70	Hγ	H3	3.4 ± 2
70	Hγ	H1	2.8 ± 2
70	Hγ	H6	2.8 ± 2
42	Hγ	H6	5.5 ± 2
68	Hβ	H5	3.3 ± 2
47	$H\alpha_1$	H6	3.1 ± 2
47	$H\alpha_1$	H7	5.0 ± 2
47	$H\alpha_2$	H6	2.9 ± 2
47	$H\alpha_2$	H7	2.9 ± 2

PRE-derived distances

Ub Residue	Ub atom	h-ubiB atom	Distance
48	O (MTSL)	H1	13.3 ± 4
48	O (MTSL)	H2	12.0 ± 4
48	O (MTSL)	H3	11.9 ± 4
48	O (MTSL)	H4	10.5 ± 4
48	O (MTSL)	H5	9.5 ± 4
48	O (MTSL)	H6	10.0 ± 4
48	O (MTSL)	H7	12.1 ± 4
48	O (MTSL)	H8	12.3 ± 4
48	O (MTSL)	H9	11.4 ± 4
36	O (MTSL)	H1	14.0 ± 4
36	O (MTSL)	H2	14.8 ± 4
36	O (MTSL)	H3	15.7 ± 4
36	O (MTSL)	H4	16.8 ± 4
36	O (MTSL)	H5	17.7 ± 4
36	O (MTSL)	H6	18.3 ± 4
36	O (MTSL)	H7	18.9 ± 4
36	O (MTSL)	H8	17.5 ± 4
36	O (MTSL)	H9	16.5 ± 4

Table S4, related to Figure 3. The results of the structure calculation for the ten best structures of the best cluster for the Ub:h-ubiB complex. Numbers in the parentheses represent standard deviations.

E_{inter}[a]	E_{vdW}	E_{elec}	E_{NOE}[b]	BSA[d]	H_{bond}[e]	Hydro[f]	Score[g]	RMSD[h]	#Viol[i]
-127.9	-14.1	-113.8	75.7	517	17.8	13	-25.7	0.45	2.3
(6.9)	(7.5)	(7.8)	(1.5)	(8)	(1.5)	(2)	(1.0)	(0.10)	(0.4)

[a] Intermolecular energy: sum of the van der Waals and electrostatic energies ($kcal \cdot mol^{-1}$)
[b] NOE energy: sum of the ambiguous and unambiguous energies ($kcal \cdot mol^{-1}$)
[d] Total buried surface area for Ub and h-ubiB ($Å^2$)
[e] Number of hydrogen bonds
[f] Number of hydrophobic contacts
[g] HADDOCK score (arbitrary units)
[h] RMSD calculated with respect to the lowest HADDOCK-score structure
[i] Number of unambiguous distances violated (out of 36 distance constraints)

Supplemental References

Becke, A.D. (1998). A new mixing of Hartree–Fock and local density-functional theories. J. Chem. Phys. *98*, 1372-1377.

Eddins, M.J., Varadan, R., Fushman, D., Pickart, C.M., and Wolberger, C. (2007). Crystal structure and solution NMR studies of Lys48-linked tetraubiquitin at neutral pH. J Mol Biol *367*, 204-211.

Lee, C., Yang, W., and Parr, R.G. (1988). Development of the Colle-Salvetti correlation-energy formula into a functional of the electron density. Phys. Rev. B. *37*, 785-789.

Neese, F. (2008). ORCA – an ab initio, Density Functional and Semiempirical program package. (University of Bonn).

Ryabov, Y., and Fushman, D. (2006). Interdomain mobility in di-ubiquitin revealed by NMR. Proteins *63*, 787-796.

Schuttelkopf, A.W., and van Aalten, D.M. (2004). PRODRG: a tool for high-throughput crystallography of protein-ligand complexes. Acta crystallographica. Section D, Biological crystallography *60*, 1355-1363.

Singh, R.K., Zerath, S., Kleifeld, O., Scheffner, M., Glickman, M.H., and Fushman, D. (2012). Recognition and cleavage of related to ubiquitin 1 (Rub1) and Rub1-ubiquitin chains by components of the ubiquitin-proteasome system. Mol Cell Proteomics *11*, 1595-1611.

Varadan, R., Assfalg, M., Raasi, S., Pickart, C., and Fushman, D. (2005). Structural determinants for selective recognition of a Lys48-linked polyubiquitin chain by a UBA domain. Mol Cell *18*, 687-698.